A comprehensive multiscale framework for simulating optogenetics in the heart

SUPPLEMENTARY INFORMATION

Patrick M Boyle[1], John C Williams[2], Christina M Ambrosi[2],

Emilia Entcheva[2], Natalia A Trayanova[1]

[1]Institute for Computational Medicine, Johns Hopkins University, Baltimore, MD, USA.
[2]Institute for Molecular Cardiology, Stony Brook University, Stony Brook, NY, USA.

Supplementary figures

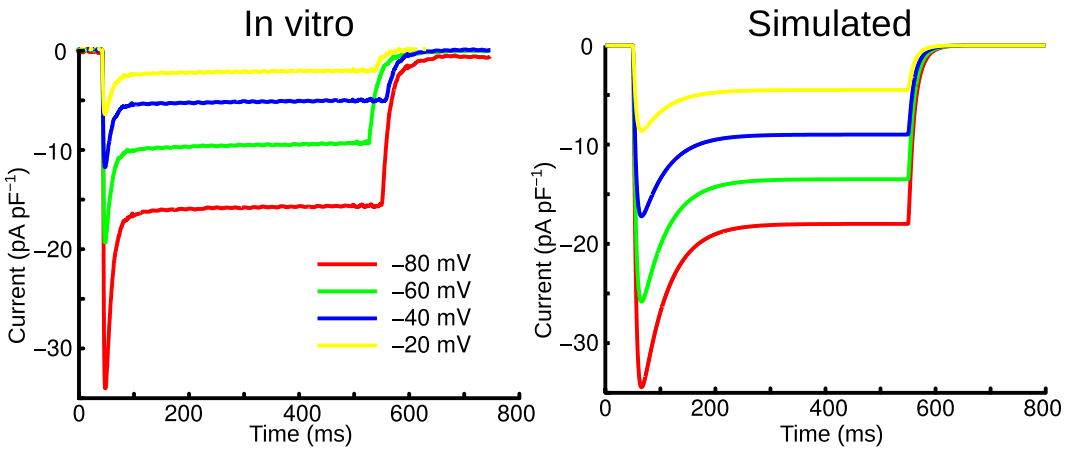

Supplementary Figure S1: **Comparison of in vitro and simulated ChR2 currents.** Light-sensitive currents were obtained with membrane voltage clamped to physiologically relevant values. Experimental values were recorded in a stable HEK-ChR2 cell line.[21] In all cases, irradiance applied was 5.5 $mW\,mm^{-2}$.

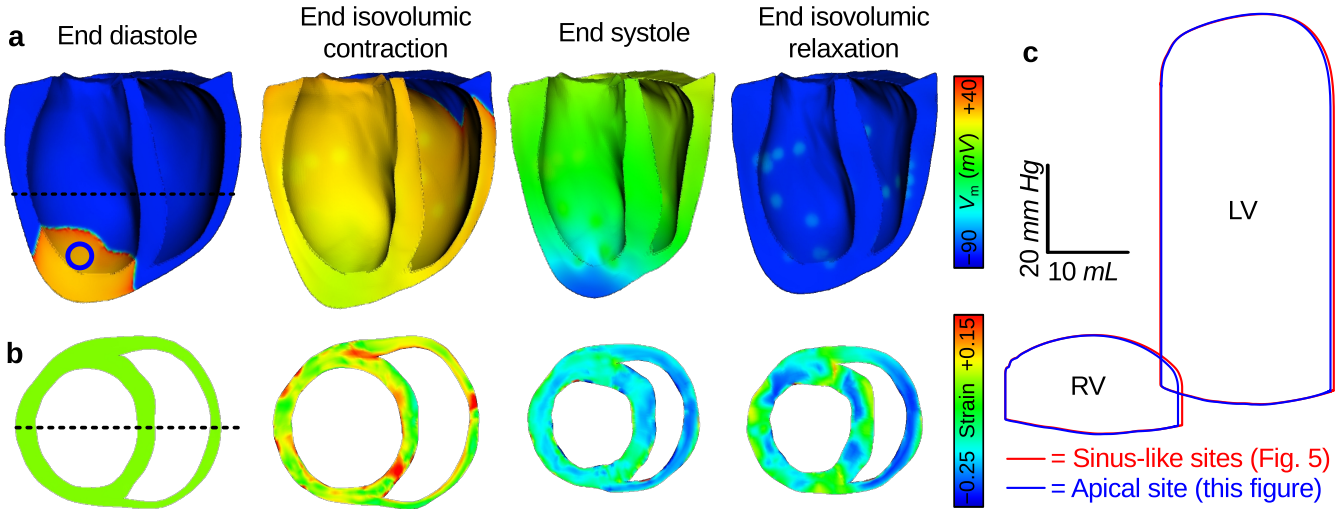

Supplementary Figure S2: **Electromechanical response to optical stimulation at LV apex.** (A&B) Long-axis membrane voltage (V_{m}) and short-axis strain profiles (unitless) during the cardiac cycle. Illumination delivered 12.8 $mW\,mm^{-2}$ to a single ChR2 delivery site (blue circle) for 10 ms at $t = 0$. See Fig. 7 legend for more details. (C) LV and RV pressure-volume loops for the photoevoked response (blue) with loops from Fig. 7 (d) superimposed for comparison.

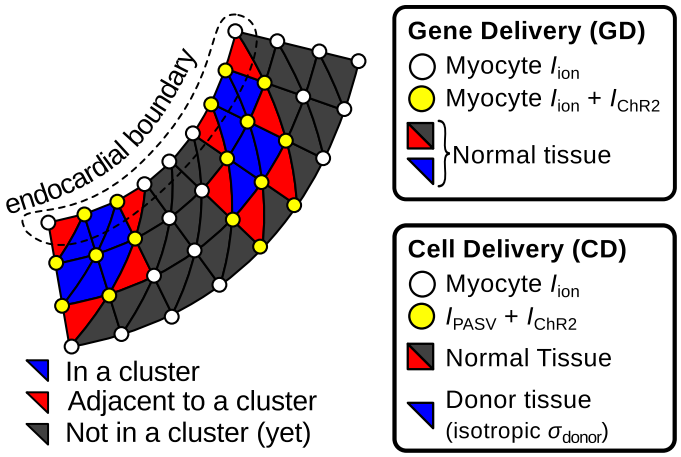

Supplementary Figure S3: **Simulated ChR2 delivery in a representative 2D schematic.** Stochastic algorithm parameters were $D = 0.25$ and $P = 0.05$. Since P was relatively low, the algorithm generated only two clusters of light-sensitive cells. Assignment of cell- and tissue-level properties to nodes (circles) and elements (triangles) for GD vs. CD is summarised. In elements tagged as light-sensitive, all constitutive nodes have ChR2-expressing membrane.

Supplementary tables

Supplementary Table S1: I_{ChR2} **model parameters**

Category	Parameter(s)	Value	Reference
C2:C1 conductance ratio	γ	0.1	[29]
Rate constants	$C_1 \rightarrow O_1$	k_1	[29]
	$O_1 \rightarrow C_1$	G_{d1}	[29]
	$O_1 \rightarrow O_2$	e_{12}	[29]
	$O_2 \rightarrow O_1$	e_{21}	[29]
	$O_2 \rightarrow C_2$	G_{d2}	[29]
	$C_2 \rightarrow O_2$	k_2	[29]
	$C_2 \rightarrow C_1$	G_{r}	[29]
Kinetic parameters	F	$0.00006 \times E_{\mathsf{e}} \times \lambda \times w_{\mathsf{loss}}$	[29]$*$
	S_0	$0.5(1 + tanh(120(E_{\mathsf{e}} - 0.1)))$	[53]
	ϵ_1	0.8535	[53]
	ϵ_2	0.14	[29]
	k_1	$\epsilon_1 \times F \times p$	[53]
	k_2	$\epsilon_2 \times F \times p$	[53]
	G_{d1}	$0.1\,ms^{-1}$	[54]
	G_{d2}	$0.05\,ms^{-1}$	[54]
	w_{loss}	$0.76 = 1/1.3$	[29]
	$e_{12,\mathsf{dark}}$	$0.011\,ms^{-1}$	[54]
	$e_{21,\mathsf{dark}}$	$0.008\,ms^{-1}$	[54]
	c_{12}	$0.005\,ms^{-1}$	[54]
	c_{21}	$0.004\,ms^{-1}$	[54]
	Φ_0	$0.024\,mW\,mm^{-2}$	[54]
	e_{12}	$e_{12,\mathsf{dark}} + c_{12} \times log_{10}(E_{\mathsf{e}}/\Phi_0)$	[54]
	e_{21}	$e_{21,\mathsf{dark}} + c_{21} \times log_{10}(E_{\mathsf{e}}/\Phi_0)$	[54]
	G_{r}	$0.004\,ms^{-1}$	[53]
	τ_{ChR2}	$1.3\,ms$	[29]
Maximum ChR2 conductance	g_{ChR2}	$2.0\,mS\,cm^{-2}$	–
Rates of change	$\partial O_1/\partial t$	$k_1 C_1 + e_{21} O_2 - (G_{\mathsf{d1}} + e_{12}) O_1$	[53]
	$\partial O_2/\partial t$	$k_2 C_2 + e_{12} O_1 - (G_{\mathsf{d2}} + e_{21}) O_2$	[53]
	$\partial C_1/\partial t$	$G_{\mathsf{r}} C_2 + G_{\mathsf{d1}} O_1 - k_1 C_1$	[53]
	$\partial C_2/\partial t$	$G_{\mathsf{d2}} O_2 - (k_2 + G_{\mathsf{r}}) C_2$	[53]
	$\partial p/\partial t$	$(S_0 - p(t))/\tau_{\mathsf{ChR2}}$	[53]

$*$: corrected from parameter value specified by Nikolic et al.[29]

Supplementary Table S2: **Simulation Details for MRI-based Human Ventricles**

Category	Parameter(s)		Value
Geometry	# degrees of freedom (nodes)		2,423,911
	# mixed-type elements		2,929,297
Conductivity ($mS\,mm^{-1}$)	endocardium & midmyocardium	σ_{iL}	0.5000
		σ_{iT}	0.1200
		σ_{iN}	0.0525
	epicardium	σ_{iL}	0.2550
		σ_{iT}	0.0775
		σ_{iN}	0.0400
Computation	# of Intel X5660 processors @2.80 GHz		48
	wall time required for to simulate 1 s		2.89 h

Supplementary Table S3: **Simulation Details for rabbit Ventricles and PS**

Category	Parameter(s)		Value
Geometry	# degrees of freedom (nodes)		547,680
	# tetrahedral elements		3,073,529
	# degrees of freedom in PS		2,232
	# cubic Hermite Purkinje elements		1,116
Conductivity ($mS\,mm^{-1}$)	throughout myocardium (rotationally isotropic)	σ_{iL}	0.1845
		σ_{iT}	0.0239
		σ_{iN}	0.0239
Purkinje-myocardial junctions (see previous papers on PS modelling[25,60])	Junctional resistance (R_{PMJ})		85 MΩ
	Junctional scaling factor (K_{PMJ})		80,000
	# ventricular nodes per PS node (n_{PMJ})		200 to 220
	PS endpoint penetration depth		10%
	PS fibre radius (r_{PS})		15 μm
	PS fibre internal conductivity (σ_{PS})		0.1 $mS\,mm^{-1}$
	PS fibre gap junction resistance (R_{gj})		100 kΩ
Computation	# of Intel E5472 processors @3.00 GHz		8
	wall time required for to simulate 1 s		2.47 hrs

Supplementary discussion

Modelling channel- and cell-level cardiac optogenetics: Our model of I_{ChR2} qualitatively matches measurements in ChR2-expressing HEK cells and it reproduces the response of light-sensitive cells to illumination. In our framework, we developed the capability to incorporate this model while representing different delivery modes. For CD, this includes a model of light-sensitive donor cells based on measurements from ChR2-rich HEK cells; the latter cells have been used successfully in cardiac optogenetics experiments.[21] The utility of CD and GD in practical optogenetic therapy has not been explored; our framework allows for such an exploration. Simulations enable side-by-side comparison of optical stimulation efficiency for gene- and cell-delivered ChR2, including spatial distribution of light-sensitive cells; this level of examination, which would be difficult to achieve in vitro, could accelerate clinical translation by identifying which ChR2 delivery modes result in the most efficient optical stimulation.

In this study, we incorporated only I_{ChR2} because it is the only photoevoked current for which there is sufficient experimental data to construct a detailed mathematical model; however, our cell-level approach could be used to model GD or CD of other opsins, such as the light-activated chloride pump halorhodopsin, which has been used experimentally to silence autorhythmic cardiomyocyte activation.[18] Similarly, we modelled donor cells with HEK cell-like properties since they have been used experimentally in the context of cardiac optogenetics;[21] however, our approach could be extended to model CD of ChR2 with other types of donor cells, such as myofibroblasts or stem cells.

Modelling spatial distribution of light-sensitive cells: Our stochastic algorithm for modelling light-sensitive cell distribution at the tissue level allows for the representation of realistic distributions of photosensitive cells. Implementation of truly heterogeneous spatial distributions is a departure from the norm in cardiac modelling, where heterogeneities are modelled with smooth gradients or disregarded altogether.[20]

Patterns of transgene expression and donor cell distribution can change in density and/or patchiness over time;[61,62] a particular ChR2 delivery, initially dense enough to result in optical

stimulus capture, might evolve towards a distribution that is more sparse, possibly resulting in decreased optical stimulation efficiency. Our approach could be extended to incorporate a time-dependent component to modelling cluster evolution.

Finally, spatial distributions of light-sensitive cells simulated with our framework could be used to design stencils for controlled ChR2 delivery to achieve matching cell cultures, thus providing an experimental/simulation tool for exploring optical stimulation efficiency. In a preliminary study, simulations of cardiac cell monolayers with CD ChR2 yielded comparable $E_{\mathsf{e,thr}}$ values to those observed in experimental monolayers with qualitatively similar light-sensitive cell distributions.[63]

Modelling illumination of the heart: Our framework incorporates an accurate model of light attenuation, which is an essential component in the accurate representation of optical stimulation. The ChR2 delivery sites in our illustrative examples are relatively small (diameters of $2\,mm$ in rabbits, $3\,mm$ in dogs, and $1\,cm$ in humans) compared to organ scale. Later in this section, we explain how the associated endocardial illumination patterns might be achieved as part of a detailed discussion on the feasibility of cardiac optical stimulation in vivo and in vitro (see: **Feasibility and energy efficiency of optical stimulation**).

Our monoexponential decay model for light attenuation has been validated for uniform illumination of localised areas, such as small regions of endocardium for ChR2 delivery sites,[39] and is suitable for analysis of many aspects of cardiac optogenetics, including optical stimulation efficiency and cell-specific targeting with focal light sources. Optical stimulation with light of different wavelengths can be simulated by adjusting the decay coefficient (δ), which is important for framework expansion since opsins other than ChR2 are controlled by different-coloured light. If observations from in vivo cardiac optogenetics experiments are found to conflict with simulation predictions due to photon backscattering effects near the illuminated surface, our representation of light attenuation could be refined to incorporate a biexponential decay model, as shown previously for green light.[64] As the field continues to evolve it may also be necessary to simulate more complex forms of optical stimulation, such as two-photon excitation of ChR2 or illumination of blood-filled atrial or ventricular cavities with red or green light to excite different opsins. In

these situations, our framework could be expanded to perform a one-time solution of the photon diffusion equation using a simple finite element scheme[65] each time the light source turns on.

Modularity and versatility of the optogenetic framework: Our framework is flexible with regards to physiological details such as species or disease state; enables selective inscription of light sensitivity in specific cell populations (e.g., PS fibres, ventricular or atrial myocytes, fibroblasts, nodal pacemaker cells, etc.); and can be implemented in any appropriate software platform. Integration of photocurrents other than I_{ChR2} is straightforward and different donor cell types can be simulated by exchanging I_{PASV} for a more detailed membrane model. The framework is also versatile in terms of the spatial distributions of light-sensitive cells in tissue. Finally, as highlighted by our demonstration of optical stimulation in an electromechanical model, our optogenetic simulation components are entirely modular; any model component that can interact with the electrophysiology module alone (e.g., mechanics, fluidics, remodelling due to disease, etc.) can also be considered in the context of cardiac optogenetics. This is particularly noteworthy for electromechanical problems, since it enables model-based analysis of possible optogenetic therapies to treat cardiac pump dyssynchrony, including targeted optical pacing as an alternative to conventional cardiac resynchronization therapy.

Feasibility and energy efficiency of optical stimulation: When considering the possibility of translating cardiac optogenetics to clinical application, it is important to consider whether in vivo optical stimulation of the heart is feasible and to assess its relative energy efficiency compared to conventional electrical stimulation. At present, optical stimulation of ChR2 is subject to numerous physical limitations. Due to the significant attenuation of blue light in both tissue and blood, the optrode tip must be proximal to the illumination target much like the tip of a pacing electrode must be in contact with the tissue to effectively stimulate. Numerous commonly-used clinical tools use catheter-based fibre optics for intravenous and intracardiac imaging (e.g., angioscopy,[66] optical coherence tomography,[67] near-infrared spectroscopy[68]). These optrodes are relatively small (3 to 8 *French*) and it is not difficult to envision how they could be adapted to illuminate instead of record. Hexagonal optrode arrays ranging from $400\,\mu m$ to $750\,\mu m$ in

diameter have been used to perform intramural optical measurements of V_{m} in Langendorff-perfused rabbit hearts;[69,70] we envision adapted versions of these devices that will be utilised for in vitro optical stimulation.

In terms of in vivo optrode access, numerous techniques developed for stimulating specific regions or structures in conventional electrophysiology will be equally useful in optical stimulation regimes. For example, optical His bundle pacing (as in Fig. 6 (c)) could be achieved by accessing the distal conduction system via the coronary sinus, as shown clinically for electrical stimulation.[46] Similarly, optical pacing from the LV endocardium (as in Fig. 5) could be accomplished by applying the Jurdham procedure,[71] although the maximal optrode radius would be approximately $3\times$ smaller than our simulated example.

Finally, as optogenetics technology continues to evolve, new strategies will be engineered to improve the clinical feasibility of optical stimulation. Efforts are already underway to modify blue light-sensitive opsins (such as ChR2) in such a way that they can be excited by longer-wavelength light (i.e., "red-shifting"), which is subject to much weaker attenuation.[17] As these developments occur, the photocurrent and light attenuation modules of our framework can be easily adapted to investigate novel optical stimulation schemes; for example, modules could be straightforwardly modified to explore the feasibility and clinical benefit of inscribing light sensitivity with red-shifted ChR2 and placing a red LED in the ventricular cavity to safely and efficiently illuminate the entire endocardium.

The relative energy efficiency of optical stimulation compared to conventional current injection is not yet completely understood. In terms of total charge delivered to the cell, it has been suggested that the optogenetic modality is inherently more optimal than conventional electrical current, especially in the context of low-amplitude, long-duration stimuli.[19] The voltage sensitivity and inward rectification properties of light-sensitive channels provide an instantaneous feedback mechanism, causing excitatory current to terminate as soon as an action potential has been initiated. Additionally, there may be major indirect gains in efficiency due to the fact that optogenetics allows for specific cell or tissue types to be targeted; for example, as shown in Fig. 6

the Purkinje system is easier to excite than bulk myocardium due to both intrinsic membrane kinetics and less significant source-to-load mismatch, assuming equivalent current densities can be achieved by targeted gene delivery to the two cell types. Ultimately, direct comparison of real energy consumption for electrical versus optical stimulation in the heart will not be possible until cardiac optogenetics experiments progress to the in vivo stage; in the interim, this is an interesting potential application for our framework.

In vitro validation of model findings: A critical aspect of model-based research is to move forward and test the mechanistic hypotheses generated by simulations. In this paper, we present illustrative examples involving whole-heart models, but the framework could just as easily be applied to simulate optical stimulation in preparations that are more easily compared with current in vitro cardiac optogenetics experiments, such as cardiac cell monolayers. Our findings regarding the relationship between optical stimulation efficiency, light-sensitive cell distribution, and ChR2 delivery mode could be validated using side-by-side comparison of in vitro and simulated monolayers with identical spatial patterns of ChR2-expressing myocytes or donor cells; model parameters could then be iteratively adjusted to incorporate new observations as they are made. A good initial test of our conclusions regarding efficiency in the PS versus well-coupled myocardium would be to compare optical excitation thresholds between isolated, light-sensitised Purkinje fibre cells and ventricular myocytes. Although the relative benefits of differential stimulation by cell-specific optogenetic targeting cannot be tested until ventricle- and/or PS-specific promoters for ChR2 delivery are developed, our conclusions could be tested by comparing optical stimulation dynamics in a cultured strand of cells versus a well-coupled tissue wedge.

Supplementary references

[60] Boyle, P. M., Veenhuyzen, G. D. & Vigmond, E. J. Fusion during entrainment of orthodromic reciprocating tachycardia is enhanced for basal pacing sites but diminished when pacing near Purkinje system end points. *Heart Rhythm* **10**, 444–451 (2013).

[61] Reimsnider, S., Manfredsson, F. P., Muzyczka, N. & Mandel, R. J. Time course of transgene expression after intrastriatal pseudotyped rAAV2/1, rAAV2/2, rAAV2/5, and rAAV2/8 transduction in the rat. *Mol Ther* **15**, 1504–1511 (2007).

[62] Wang, X. *et al.* Dynamic tracking of human hematopoietic stem cell engraftment using in vivo bioluminescence imaging. *Blood* **102**, 3478–3482 (2003).

[63] Boyle, P. M., Williams, J. C., Entcheva, E. & Trayanova, N. A. Spatial distribution of channelrhodopsin-2 affects optical stimulation efficiency in cardiac tissue. *Heart Rhythm* **9**, S182 (2012).

[64] Baxter, W. T., Mironov, S. F., Zaitsev, A. V., Jalife, J. & Pertsov, A. M. Visualizing excitation waves inside cardiac muscle using transillumination. *Biophys J* **80**, 516–530 (2001).

[65] Bernus, O., Wellner, M., Mironov, S. F. & Pertsov, A. M. Simulation of voltage-sensitive optical signals in three-dimensional slabs of cardiac tissue: application to transillumination and coaxial imaging methods. *Phys Med Biol* **50**, 215–229 (2005).

[66] Honda, Y. & Fitzgerald, P. J. Frontiers in intravascular imaging technologies. *Circulation* **117**, 2024–2037 (2008).

[67] Bezerra, H. G., Costa, M. A., Guagliumi, G., Rollins, A. M. & Simon, D. I. Intracoronary optical coherence tomography: A comprehensive review clinical and research applications. *JACC Cardiovasc Interv* **2**, 1035–1046 (2009).

[68] Madder, R. D., Steinberg, D. H. & Anderson, R. D. Multimodality direct coronary imaging with combined near-infrared spectroscopy and intravascular ultrasound: Initial US experience. *Catheter Cardiovasc Interv* **81**, 551–557 (2013).

[69] Hooks, D. A., LeGrice, I. J., Harvey, J. D. & Smaill, B. H. Intramural multisite recording of transmembrane potential in the heart. *Biophys J* **81**, 2671–2680 (2001).

[70] Byars, J. L., Smith, W. M., Ideker, R. E. & Fast, V. G. Development of an optrode for intramural multisite optical recordings of V_m in the heart. *J Cardiovasc Electrophysiol* **14**, 1196–1202 (2003).

[71] Elencwajg, B. *et al.* The Jurdham procedure: endocardial left ventricular lead insertion via a femoral transseptal sheath for cardiac resynchronization therapy pectoral device implantation. *Heart Rhythm* **9**, 1798–1804 (2012).